ACS OMEGA

http://pubs.acs.org/journal/acsodf

Article

Anew Synthetic Polymers Based on Polyaniline for Dual-Functional Applications: Photoelectrochemical Water Splitting and Antibacterial Activities

Reem M. Abdelfattah, Mohamed Shaban, Fatma Mohamed,* Ahmed A.M. El-Reedy, and Hanafy M. Abd El-Salam

Cite This: *ACS Omega* 2021, 6, 20779−20789

Read Online

ACCESS | Metrics & More | Article Recommendations | Supporting Information

ABSTRACT: Polysulfanilic acid has a low efficiency for the photoelectrochemical (PEC) production of H_2 from water splitting due to high recombination rate of charge and low electrical conductivity. Therefore, polyaniline was doped with polysulfanilic acid to form a copolymer and a blend to enhance its PEC heterogeneous catalytic performance. This was achieved through the improvement of visible light absorption and charge carriers' separation property. Herein, nine polymer samples of polysulfanilic acid were synthesized by oxidative polymerization. The structural, morphological, and optical properties of the synthesized polymeric materials were investigated. Interestingly, these polymer samples had multifunctional applications regarding their hydrogen generation efficiency. Photoelectrodes of different compositions from pure and blended polymers were prepared and used for the PEC solar hydrogen production from water. Different PEC parameters including the oxidant role, monochromatic illumination wavelength, and electrode reusability were optimized toward the efficient hydrogen generation. Moreover, the PEC performance was evaluated using key indicators such as photocurrent density, conversion efficiency, and the number of hydrogen moles. The number of hydrogen moles was quantitatively estimated to be 140.4, 160.2, and 300 μmol/h·g at −1 V for the polymer, copolymer, and polymer blend, respectively, in the presence of APS + $FeCl_3$ as an oxidant. Further, other samples of polymers showed antimicrobial properties against different species of bacteria. Hence, the present study may provide a cost-effective method to produce solar hydrogen fuel from water.

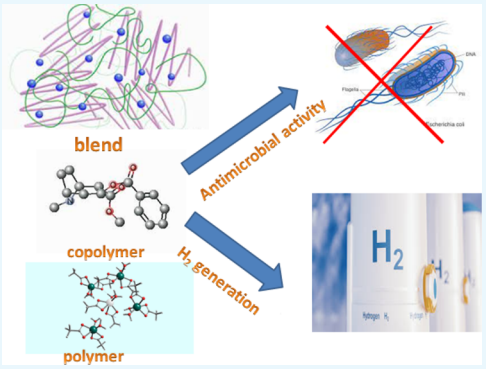

1. INTRODUCTION

Environmental remediation and engineering require highly efficient and chemically stable materials. Conducting polymers (CPs) have achieved considerable interest for various applications including water splitting, solar cells, bacterial disinfection,[1−5] bioremediation, and energy generation depending on their unique properties. CPs are cheap, easily prepared, activated by visible light, environment-friendly, have appropriate optical bandgap, long-lived, and energy efficient.[6] Hydrogen is one of the greenest futures competitive to fossil fuels due to crucial advantages including economic cost, high efficiency, eco-friendliness, renewability, and availability. It is considered a promising fuel that may solve the critical energy and environmental problems.[7,8]

There are various hydrogen-producing technologies from water. For their environmental and economic benefits, photocatalytic and photoelectrochemical (PEC) water splitting methods were recommended over the others as they can be carried out using artificial light or sunlight as the energy source.

The prerequisite for PEC is the development of visible-light-active photocatalysts. To design effective PEC catalysts, strategic materials are needed to be used as inexpensive, visible light active, eco-friendly, long-lived, and energy-efficient photocatalysts to promote the hydrogen evolution reaction (HER). CPs have an extended p-conjugated electron system. Upon visible light excitation, they are powerful electron donors and strong full transporters. They have environmental, electrical, optical, and electrochemical properties and can be synthesized chemically and electrochemically. In addition, due to their sufficient bandgap, they have high charge carrier mobility and strong absorption in the visible spectrum.[9−11] One of the common CPs, commercially available, light-sensitive poly sulfanilic acid (SA), is used as a good catalyst in the water splitting owing to its synthesis of sulfonic acid ring-substituted polyaniline with high conductivity and good solubility by the reaction. Polysulfanilic acid is represented not

Received: April 4, 2021
Accepted: July 8, 2021
Published: August 6, 2021

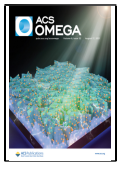

only as an electron donor but also a good hole acceptor. Therefore, this material is a good candidate for improving the charge-transfer efficiency, consequently enhancing the photocatalytic performance of photocatalysts.[12]

The copolymers of SA with derivatives containing polyaniline are well-synthesizing materials for the copolymer and blend photocatalyst to produce H_2 from water splitting under visible/solar light. Heterogeneous photocatalysis has become a low-cost and eco-friendly target well studied in wastewater treatment.[13]

Electroactive conductive polymers are of great significance in various technologies such as displays, solar cells, gas sensors, and actuators. PANI is one of the dopant polymers that has significant effects on enhancing the photocatalytic performance of other polymers by stimulating the separation of electron and hole pairs and reducing the recombination of generated electrons and charges holes.[14−16] The presence of dopants and the doping levels have effects on the physical properties of CPs. The doping level can be easily changed by a chemical reaction at room temperature, which provides a simple technique to promote its use in energy applications. Semiconductor doping is a key parameter to control the spectral and electrical properties of materials, making its application in PEC cells feasible. The basic principle of doping in π-conjugated polymer semiconductors is the same as that of conventional inorganic semiconductors. Furthermore, a combination of pure polyaniline with other photocatalysts such as polysulfanilic acid has been evaluated as antimicrobial.

In the present work, we report for the first time a novel photoelectrocatalyst containing polymer PS/APS + $FeCl_3$ (sample I), copolymer PS/APS + $FeCl_3$ (sample II), and polymer blend PS/APS + $FeCl_3$ (sample III). Polymer PS/APS (sample IV), copolymer PS/APS (sample V), polymer blend PS/APS (sample VI), polymer PS/$FeCl_3$ (sample VII), copolymer PS/$FeCl_3$ (sample VIII), and polymer blend $FeCl_3$ (sample IX) were fabricated via chemical oxidative polymerization. Different characterization instruments have been used to investigate the physical and chemical properties of the prepared samples. The PEC performance was evaluated in terms of photogenerated current density (J_{ph}), conversion efficacy, number of evaluated hydrogen moles, electrode stability, and reusability. Also, the effect of wavelength of the monochromatic light was investigated and optimized. Moreover, the antimicrobial activities of these photocatalysts for different species of microbes were investigated.

2. RESULTS AND DISCUSSION

2.1. Molecular Weight Determination GPC Studies. The GPC analysis data for the obtained products of SA oxidation with APS under the mention experimental conditions are as follows: M_n = 3225, M_w = 3301, M_p = 3388, M_z = 3378, and M_z + 1 = 3452 in daltons, and polydispersity is 1.024. These data reveal that the obtained products are of low molecular weight.

2.2. Characterizations of the Obtained Polymers. *2.2.1. UV Spectroscopy.* The UV spectra of three polymer samples prepared in the presence of APS only are presented in Figure 1. Moreover, the other polymer samples are presented in Figures S1 and S2. In Figure 1, it is clear that the absorption band at 270 nm in the case of both SA oligomer and its copolymer with aniline is strong and sharp. This band can be attributed to $\pi-\pi^*$ transition (E2-band) of a benzene ring and B-band ($A_{1g}-B_{2u}$), respectively. This confirms the absorptions

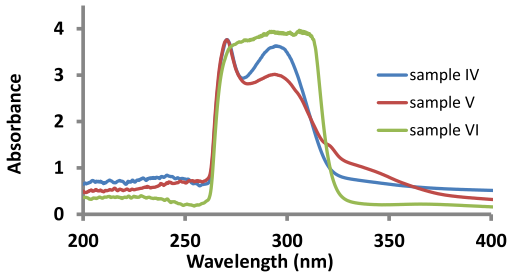

Figure 1. UV spectra of three polymer samples IV, V, and VI.

in polyaniline. Also, the broad absorption band in the case of blend in the range 270−310 nm indicates the difference between the three polymer samples in structure.

The IR absorption bands of samples prepared in the presence of APS only are presented in Figure 2. In addition,

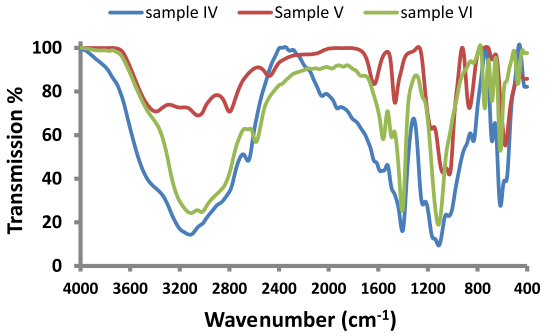

Figure 2. IR spectra of three polymer samples IV, V, and VI.

the other polymer samples are presented in Figures S3 and S4. Figure 2 shows a coincidence in bands for three materials, which confirms the interaction between SA and aniline in products. The absorption band refers to the asymmetric stretching vibration of S═O appearing at 1406, 1466, and 1407 cm^{-1} in the case of SA oligomer, copolymer, and blend, respectively. The shift in the case of copolymer confirms the chemical bonding between SA and aniline. The reset characteristic bands for other bonds such as C═C and/or C═N (1582, 1634, and 1560 cm^{-1}) and bonded OH (3117, 3393, and 3768 cm^{-1}) are present.

2.2.2. Structural and Morphological Studies. The presented XRD patterns in Figure 3 indicate that the prepared three polymer samples are polycrystalline in nature. The positions of the peaks are observed in the range of 5−65° on

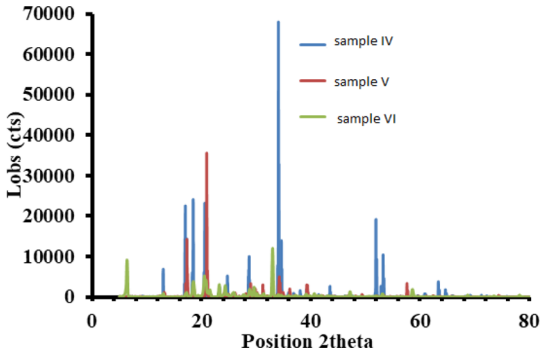

Figure 3. XRD patterns of three polymer samples IV, V, and VI.

https://doi.org/10.1021/acsomega.1c01802
ACS Omega 2021, 6, 20779−20789

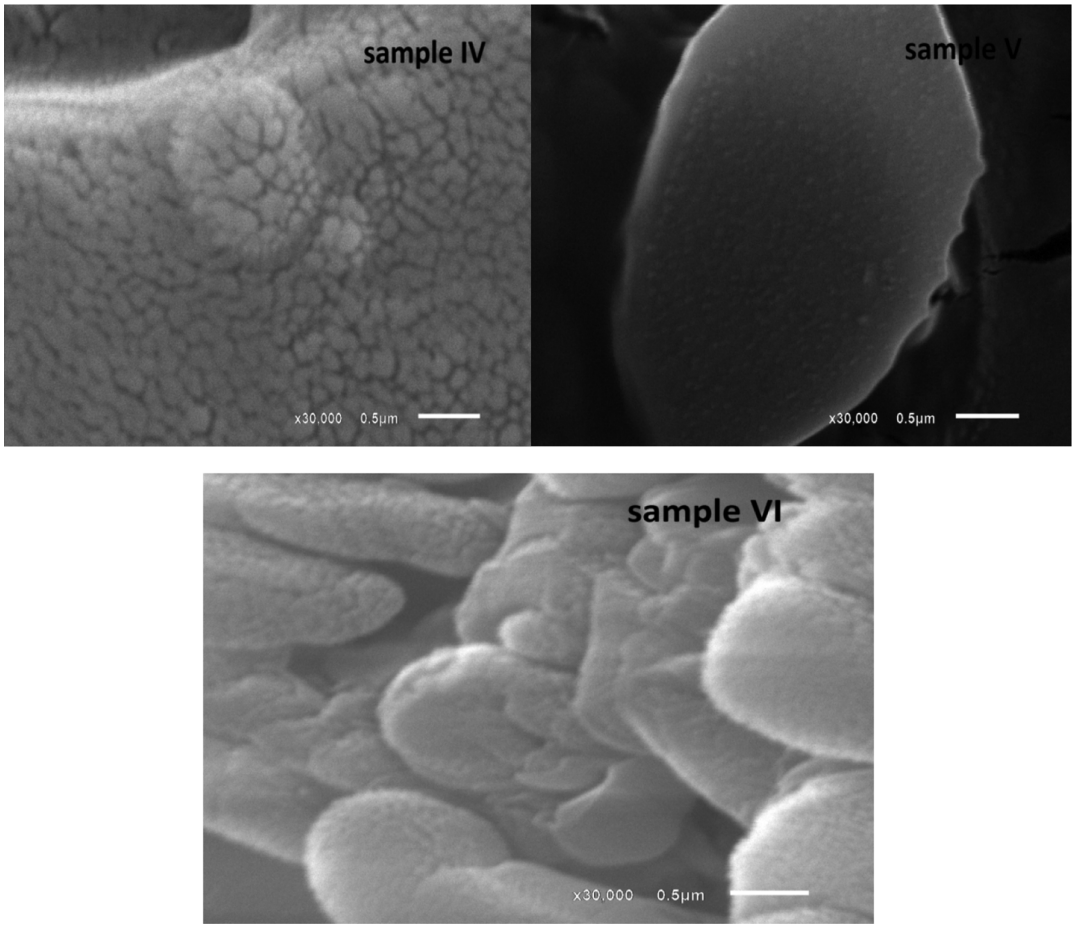

Figure 4. SEM images of three polymer samples IV, V, and VI.

the 2θ axis with different intensities, which refer to the difference of structures between the three samples.

The SEM images of the investigated samples are present in Figure 4. Moreover, the other polymer samples are presented in Figures S5 and S6. Figure 4 shows different surface morphologies between the three samples. In the case of SA oligomers, the particles are similar in shape, closed, and have identical dimensions. The surface of the copolymer seems to be nonporous, and their particles are compacted with small size. The surface of the blend is heterogeneous and has pores of varying dimensions. Also, the particles have a large size than the copolymers.

2.2.3. Optical Properties. All prepared polymer samples were introduced to optical studies, but the best data observed to three samples. The polymer samples with good optical properties are sample I, sample II, and sample III.

Optical spectroscopy is a crucial technique for understanding the conductive state corresponding to the absorption band of the state between and in the space of the conductive polymer.[17] Figure 5 illustrates the measured UV−vis absorption spectra for sample I, sample II, and sample III. Sample III shows stronger absorption than sample I and sample II. A red shift is observed in the absorption spectra following the order sample III > sample II > sample I. A strong absorption band was observed in the UV region for all samples.

The spectrum has a broad one at 380 nm and other abroad above 700 nm. The first peak was related to the presence of monomer moiety, while the second peak was related to the benzenoid group and lone pair of electrons of nitrogen. This in turn leads to $\pi-\pi^*$ interactions of the molecule.[18,19]

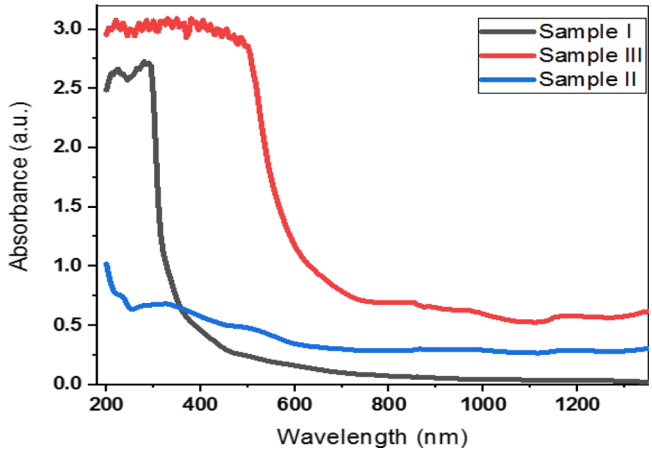

Figure 5. Absorbance spectra of samples I, II, and III.

UV−visible absorbance spectra in Figure 5 illustrate the values of the optical bandgaps of samples I, II, and III. Based on the Tauc relation, we can utilize the absorption values (A) and absorption coefficient (α_A) according to eq 1[20]

$$\alpha_A E_{ph} = A(E_{ph} - E_g)^{1/2} \quad (1)$$

where $E_{ph} = h\nu$ and E_g are for the photon energy and bandgap energy, respectively. The values of α_A are obtained from eq 2[21]

https://doi.org/10.1021/acsomega.1c01802
ACS Omega 2021, 6, 20779−20789

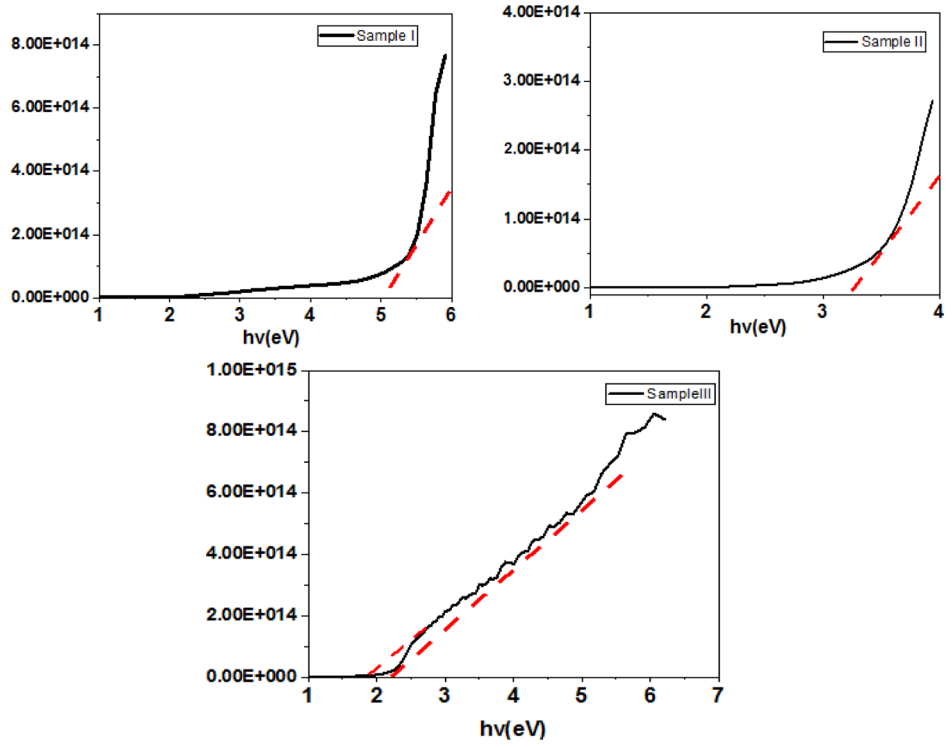

Figure 6. $(\alpha h\nu)^2$ vs $h\nu$ for energy gap calculation of sample I, sample II, and sample III.

$$\alpha_A = 2.303 \times 10^3 A\beta/lC_p \quad (2)$$

where β, l, and C_p are the material density, quartz cell width (1 cm), and suspended material concentration, respectively.

The energies of bandgap were determined by inferring the linear portion of $(\alpha_A E_{ph})^2 - E_{ph}$ plot with the E_{ph} axis, which is shown in Figure 6. They were estimated to be 5, 3.2, and 2 eV for samples I, II, and III, respectively. Due to the exclusion principle, this is a shift in the optical absorption band position, a broadening in the bandgap and the intensive absorbance of the visible light photons of the copolymer and blend as compared to the polymer. Under sunlight illumination, these parameters will simplify the electronic transitions and provide more electron/hole pairs. Hence, these samples can be used as a qualified photocatalyst for the PEC H_2O splitting.

2.3. PEC Properties of the Prepared Samples. An electrochemical potentiostat was used for photocatalytic measurement of hydrogen production (CHI660E, USA). The PEC current density−voltage ($J_{ph}-V$) and the current density−time ($J_{ph}-t$) behaviors were measured. The $J_{ph}-V$ responses were measured using a cell with a standard three-electrode configuration. The all photoelectrodes (PS/APS, PS/$FeCl_3$, PS/APS + $FeCl_3$, copolymer PS/APS, copolymer PS/$FeCl_3$, copolymer PS/APS + $FeCl_3$, polymer blend PS/APS, polymer blend PS/$FeCl_3$, and polymer blend PS/APS + $FeCl_3$) were used as the working photoelectrodes, while the Ag/AgCl electrode was used as the reference electrode, and a platinum sheet was used as the counter electrode. A light illumination of 100 mW·cm^{-2} is adjusted using a 500 W mercury−xenon light source (Newport, MODEL: 66926-500HX-R07) provided with a series of ultraviolet and visible optical filters. The working photoelectrode was fixed in the PEC cell containing the 0.3 M KOH solution and facing the lamp.

2.3.1. Effect of Photocatalyst Composition and White Light Illumination. Optimization of the photocatalyst composition is the main target for the efficient PEC H_2 generation. Therefore, we measured the PEC characteristics for the nine electrodes to evaluate their efficiencies for PEC water splitting, Figure 7a−c. The $J_{ph}-V$ curves, Figure 7a, were obtained with a sweeping voltage rate of 1 mV/s using the 0.3 M KOH (100 ml) solution at 25 °C under white light illumination. In our findings, the current density was produced from the polymer blend (sample III) and gives the highest value (60 mA/cm^2@-1 V), whereas that for the polymer itself (sample I) gives the smallest value (50 mA/cm^2@-1 V). To explore the PEC performance of these samples, the $J_{ph}-V$ curves, Figure 7b, were measured under the same conditions but in the dark. The dark current densities were 5 mA/cm^2@-1 V for the polymer blend PS/APS + $FeCl_3$(sample III) and 18 mA/cm^2@-1 V for the polymer PS/APS + $FeCl_3$(sample I). Figure 7c shows the values of current densities for the nine samples in the dark and under white light illumination at −1 V. The obtained results indicate that all of these photocatalysts could split water under visible light conditions than in dark conditions, Figure 7b,c. That is, there are sufficient amounts of electrons and holes as a result from the absorbed incident visible light. Then, the generated electrons and holes migrated to the photocatalyst surface to produce H_2 and O_2 from water.

In general, the values of photocurrent density for all samples are significant and effective due to the presence of π-orbital overlap in their backbone that produces delocalized π-electrons responsible for their photoelectric properties. These electrons support the separation efficiency of photogenerated charge carriers which in turn improve the photocatalytic performance. The blend and copolymer had a higher efficiency in PEC than the polymer itself because copolymers contain both monomer types within a single polymer chain, whereas polymer blends are made via mixing techniques (combination of multiple homopolymers, which generally occurs after synthesis). The addition of polyaniline to another chain improves PEC

https://doi.org/10.1021/acsomega.1c01802
ACS Omega 2021, 6, 20779−20789

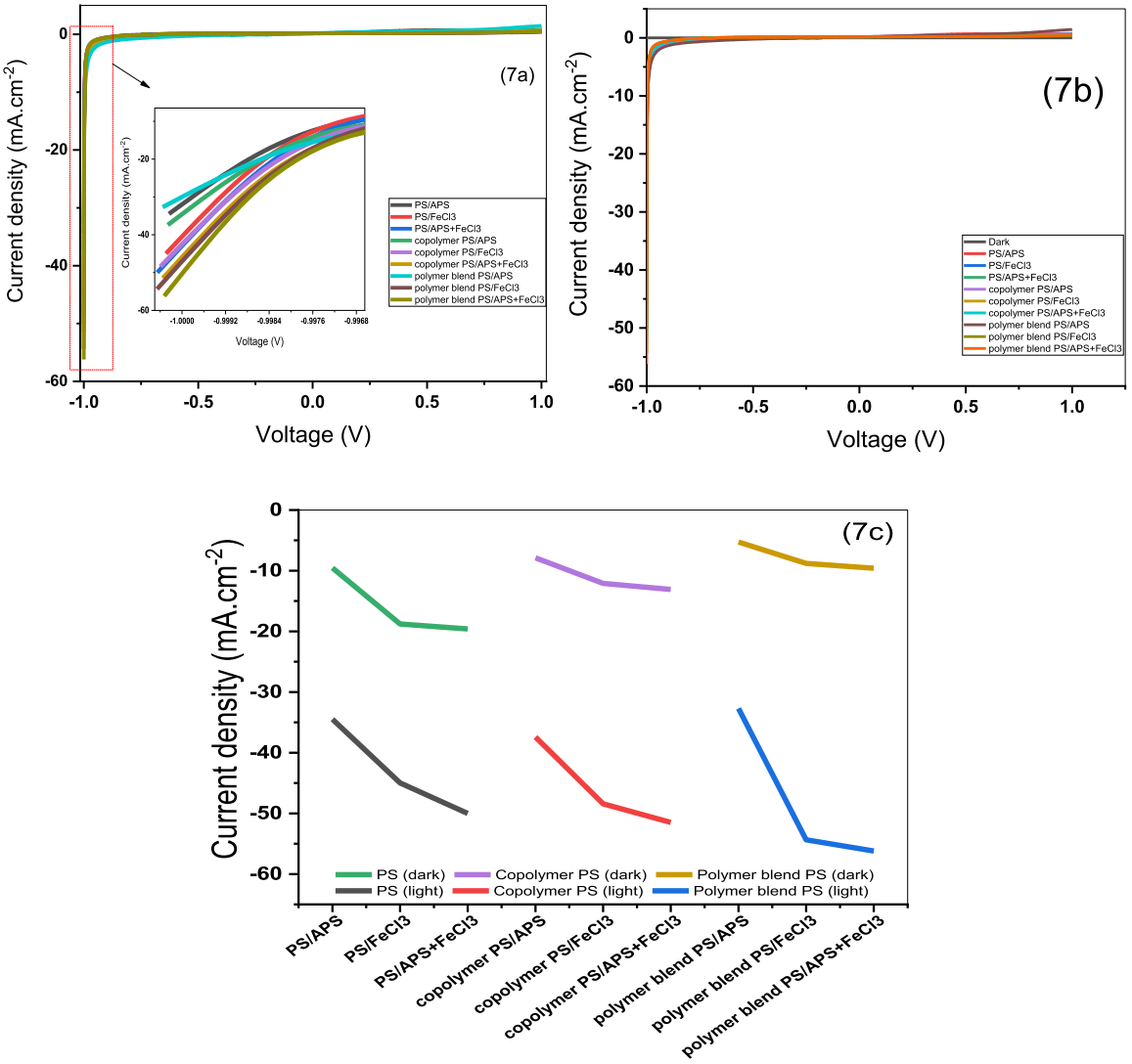

Figure 7. (a–c) J_{ph}–V curves of all samples in the dark and under white light illumination.

hydrogen generation. Polyaniline has a significant role in hydrogen production, which is represented in many factors. To begin with, hydrogen's interaction with doped PANI implies that hydrogen interacts with the charged amine group of doped PANI, forming a bridge between nitrogen atoms on two chains.

Second, it was attributed to conducting PANI's peculiar metallic electronic properties. These characteristics, combined with the molecular sieving caused by doping, undoping, and redoping, result in micropores in the polymer structure, which are advantageous for hydrogen generation.[22,23] It was noticed that the blend had higher efficiency than the copolymer; this difference in efficiency was due to the presence of polysulfanilic acid in copolymer structure, which will decrease the quinoid structure in polyaniline, thereby decreasing the electron density. While in the blend structure, the delocalized electron improved and the electron density will also increase.

Under white light exposure, it was noticed that the current densities of different samples containing $FeCl_3$ and APS as oxidants are higher in values than those of samples not containing $FeCl_3$. This can be due to the existence of the oxidants and their essential effect on improving the electrical property and conductivity of the polymers, in addition to their effect on the reaction rate. This behavior can also attribute to the structural difference between the two oxidizing agents and their interaction with monomers during the chemical synthesis and their morphologies. Ferric chloride ($FeCl_3$) as an oxidant has achieved slightly lower resistance and higher conductivity compared to the other oxidizing agent ($N_2H_8S_2O_8$).[24]

Another explanation for the increase of photocurrent of blends and copolymers than that of polymers only was ascribed to the ability of polyaniline to support both negative and positive charge carriers due to the characteristic existence of conjugated π electrons within the polyaniline backbone, which allows rigid and planar conjugative moiety for a great charge transport property along the chains. Also, intramolecular charge transfer (ICT) between donor and acceptor units could stimulate the photocurrent under light irradiation in addition to the generation of the high density of charge carrier, which provides the characteristics of high photocurrent generation in the copolymer and blend.[25,26]

2.3.2. Reusability and Stability of Photoelectrodes. Recycling experiments of the photocatalysts were carried out to analyze the stability of the synthesized materials during water splitting processes. Figure 8a–c shows the PEC behaviors for 10 reusability cycles of the photoelectrodes I,

https://doi.org/10.1021/acsomega.1c01802
ACS Omega 2021, 6, 20779–20789

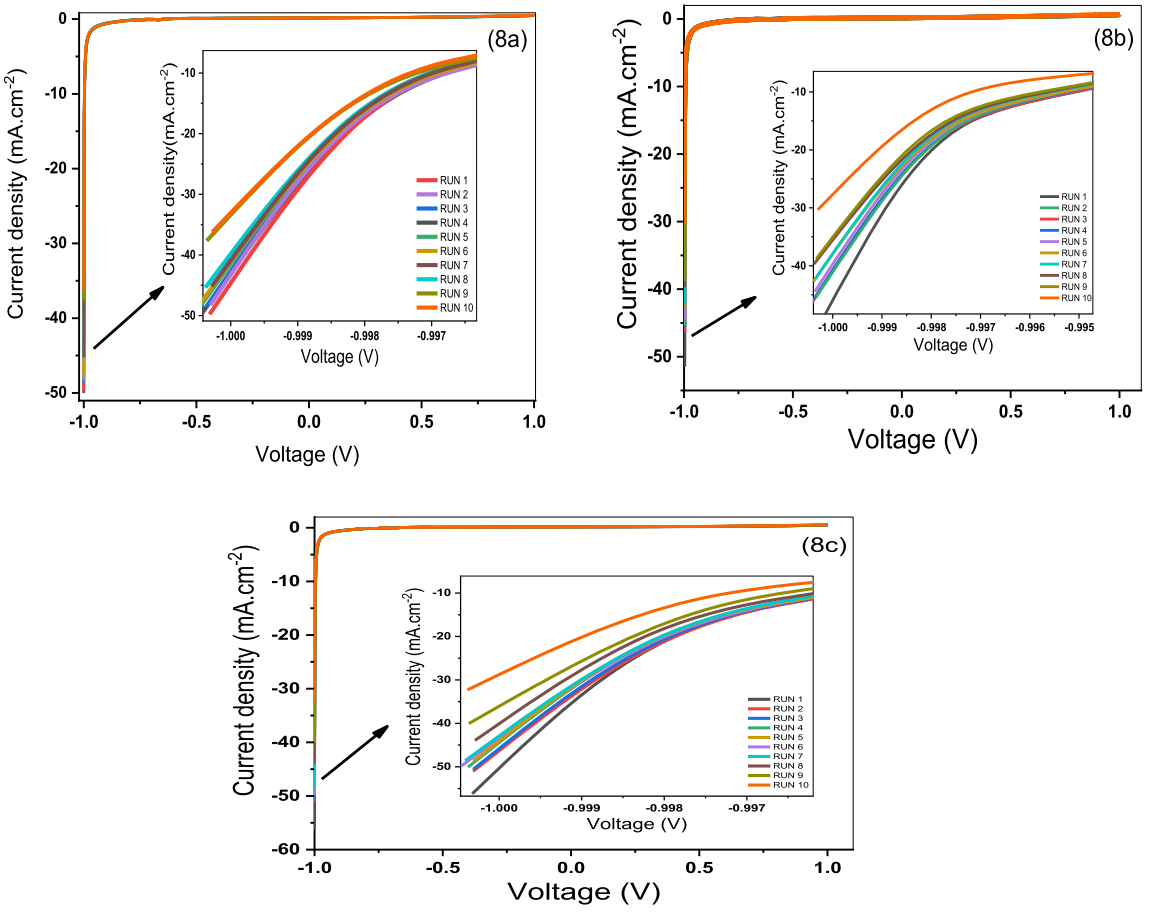

Figure 8. (a–c) Reusability of the photoelectrodes I, II, and III for 10 runs under white light conditions.

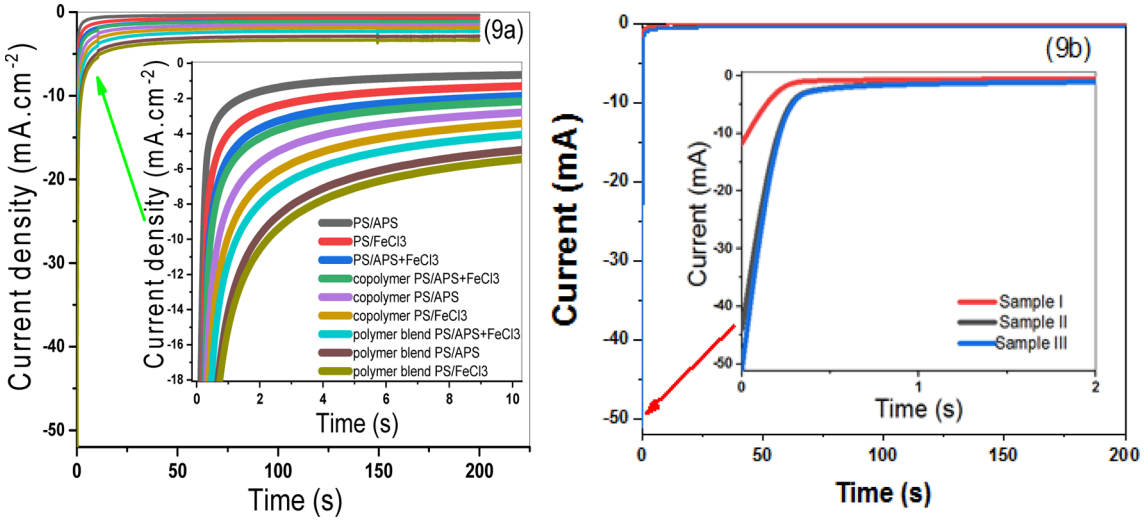

Figure 9. Current density–time characteristics for (a) all electrodes and (b) electrodes I, II, and III.

II, and III in the 0.3 M KOH electrolyte. The current density was decreased from 50 to 37 mA/cm^2 for electrode I, from 53 to 30 mA/cm^2 for electrode II, and from 65 to 34 mA/cm^2 for electrode III. This indicates that the electrodes reserve 75, 56, and 53% of their initial performance after 10 runs, which confirm the stable PEC performance of these electrodes.

The stability of the photoelectrodes was also investigated by measuring the J_{ph} vs the exposure time at a constant voltage. Figure 9a shows the J_{ph}–t curves for the nine photoelectrodes and Figure 9b for the photoelectrodes I, II, and III. From Figure 9a,b, with increasing time, there was a significant decline in J_{ph} from 52 to 4.2 mA/cm^2 of the synthesized polymer, which was oxidized in the presence of two oxidants (APS + $FeCl_3$). For t > 0.5 s, there was a steady state at a current density value of 4.2 mA·cm^{-2}. The noticeable decline in the J_{ph} values during this short time, 0.5 s, was attributed to minimal corrosion that happens as a result of the electrolyte's first reaction.[27,28]

https://doi.org/10.1021/acsomega.1c01802
ACS Omega 2021, 6, 20779–20789

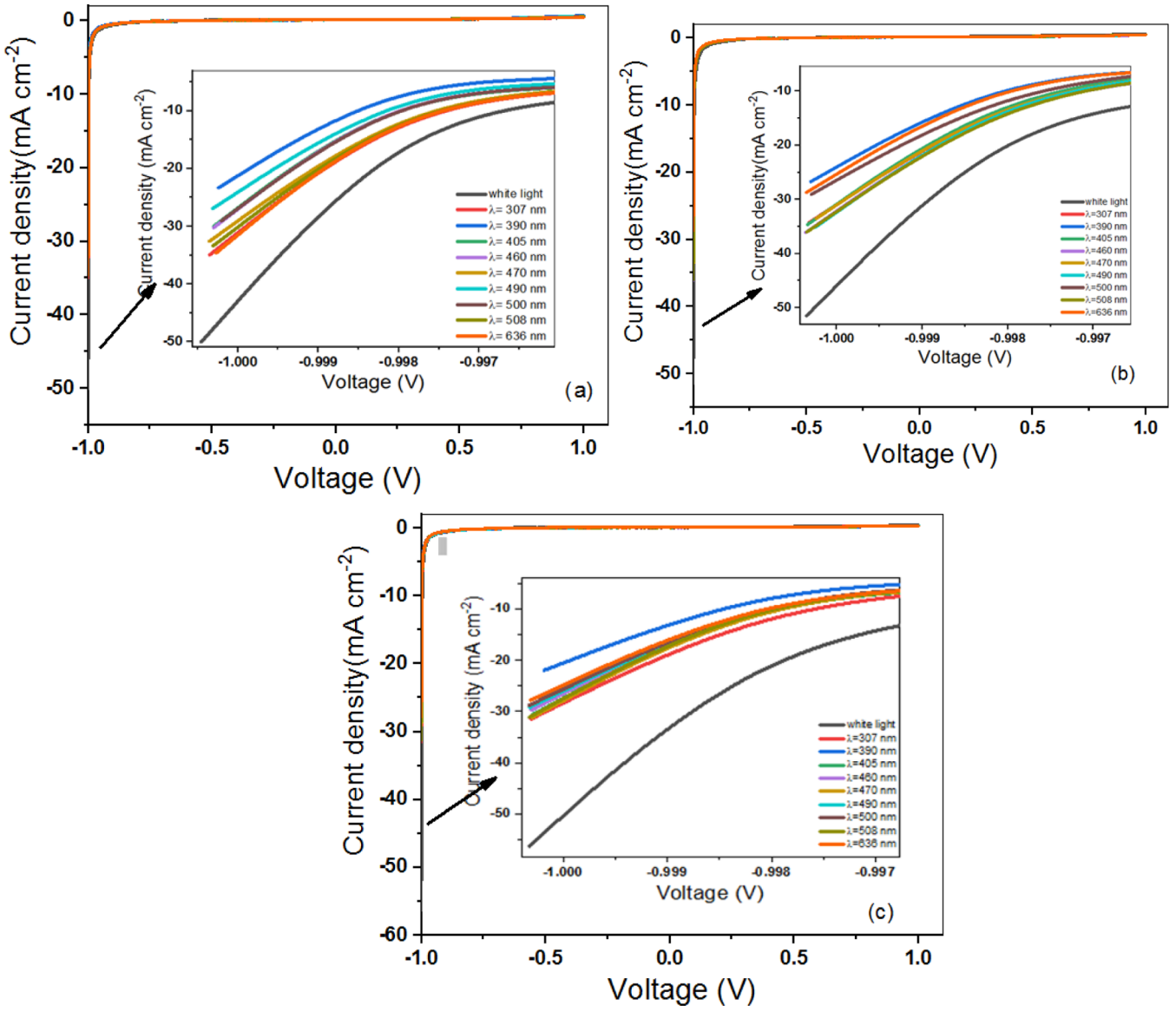

Figure 10. J_{ph}−V behaviors at different wavelengths and 25 °C using the 0.3 M KOH electrolyte and the electrodes I (a), II (b), and III (c).

The number of resultant H_2 moles during time (t) was calculated using the electrolysis law of Faraday (eq 3)[29]

$$H_2\ (\text{moles}) = \int_0^t J_{ph} \frac{dt}{F} \tag{3}$$

Based on the J_{ph}−t characteristic, the photocatalytic hydrogen output rates were 140.4, 160.2, and 300 μmol/h·g at −1 V in the 0.3 M KOH electrolyte for sample I, sample II, and sample III, respectively.

2.3.3. Effect of Optical Filters and Calculation of Conversion Efficiencies. To illustrate the effective portion of the solar spectrum that is working in all samples, both J_{ph}−V characteristics and IPCE values were recorded at different monochromatic wavelengths and are reported in Figures 10a−c.

First, the PEC reaction is started by light absorption to excite electron−hole pairs, followed by their separation into free charges, which ultimately drive redox reactions. The amount of light that a photocatalyst absorbs and the number of charges it can generate are determined by the overlap of its absorption spectrum with the irradiance spectrum of the light source.

The PEC behaviors for electrodes I, II, and III were measured under monochromatic light illuminations utilizing a group of optical filters from 307 to 636 nm, Figure 10a−c. The behaviors of the photoelectrodes and their light absorption capabilities were related to the nature of the photoelectrodes and their photoresponses to a wide portion of the visible sunlight. The most effective wavelength was 307 nm for electrode I, 405 nm for electrode II, and 307 nm for electrode III.

Also, the improved solar absorption of the photoelectrodes and their efficient application for H_2 generation from H_2O has been demonstrated by measuring incident-photon-to-current-efficiency (IPCE) at a constant applied potential of −1 V. IPCE was estimated at a constant potential under a monochromatic light for determining the number of participating charge carriers to the generated photocurrent per incident photon. Using the power density (P (mW/cm^2)) and the wavelength (λ (nm)) of the monochromatic light, the IPCE is calculated using the following eq 4[30,31]

https://doi.org/10.1021/acsomega.1c01802
ACS Omega 2021, 6, 20779−20789

$$\text{IPCE}\ (\%) = 1240 \cdot \frac{J_{ph}}{\lambda \cdot P} \cdot 100 \quad (4)$$

The obtained values of the IPCE@-1 V versus the incident wavelength are presented in Figure 11. The IPCE for

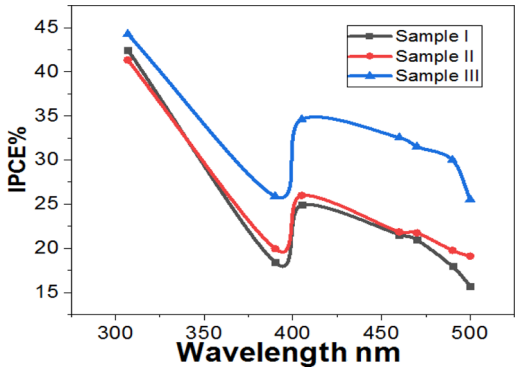

Figure 11. IPCE % vs the monochromatic wavelength at −1 V for electrodes I, II, and III.

electrodes I, II, and III have a relevant efficiency at all wavelengths, especially in the UV/visible light region. The maximum IPCE values for photoelectrodes I, II, and III were ∼46, 44, and 42% at 307 nm, respectively. These results are in agreement with the optical absorption of the samples in the UV/vis region.

2.4. Antimicrobial Activities. The three prepared SA-based polymers are effective against Gram-positive bacteria (*Bacillus subtilis* ATCC 6633 and *Staphylococcus aureus* ATCC 35556), Gram-negative bacteria (*E. coli* ATCC 23282 and *Pseudomonas aeruginosa* ATCC 10145), yeast (C 3669), and filamentous fungus (*Aspergillus niger* ATCC 16404), and the data are listed in Table S7. Our findings showed that, with the exception of SA oligomers, all polymer samples studied are biologically active against all microorganisms studied. The antibacterial activity of SA oligomers is enhanced by copolymerization with aniline. Therefore, only the polymer samples contained in PANI were measured for MIC, and the data are summarized in Table S8. The estimated MIC of the copolymer and the blend is 625 ppm; except for *Candida albicans*, the MIC of the blend is 312.5 ppm. Generally speaking, chemicals will penetrate the cytoplasm of microorganisms and destroy the genetic proteins in the cells. Therefore, this will lead to the death of microorganisms. Chemicals can generally be divided into one of the two categories: oxidizing and non-oxidizing. Oxidizing fungicides include chlorine, chlorine dioxide, bromine, ozone, and so forth, and non-oxidizing fungicides mainly include chlorophenol, glutaraldehyde, quaternary ammonium salts, and isothiazolinone. This polymer material can be classified as a non-oxidizing biocide found in our previous work.[4] Finally, the obtained values of J_{ph} and IPCE of this work are higher than the previously obtained for many photoelectrodes as shown in Table 1. This result confirmed that these photoelectrodes are the superiors for PEC water splitting under visible light irradiation.

2.5. Mechanism. As mentioned above, the light absorption capacity of the photocatalyst and the separation of the photogenerated e^-/h^+ pairs are the key factors for hydrogen generation. During the light excitation, the holes are generated at polysulfanilic acid. Then, the excited electrons are

Table 1. Comparison of the PEC Performance Parameters of the Present Work with the Previously Reported Data-Based PEC Catalysts

photocatalyst	energy gap	current performance	electrolyte	refs
polyaniline/PbS core−shell	1.41 and 2.79 eV	J_{ph} = 4.6 mA/cm^2 at 1 V, IPCE % = 36.5%@390 nm and 35.2%@405 nm	0.35 M Na_2SO_3	M. Rabia, H. S. H. Mohamed, M. Shaban, S. Taha, Preparation of polyaniline/PbS core−shell nano/microcomposite and its application for photocatalytic H_2 electrogeneration from H_2O. *Sci. Rep.* **2018**, *8*, 1107
2 min-Au/PANI/ITO	2.25 eV	J_{ph} = 2.9 mA/cm^2@1 V; IPCE = 18.7% at 390 nm	0.3 M $Na_2S_2O_3$	M. Rabia, M. Shaban, A. Adel, and A. A. Abdel-Khalieke, Effect of Plasmonic Au Nanoparticles on the Photoactivity of Polyaniline/Indium Tin Oxide Electrodes for Water Splitting. *Environ. Prog. Sustainable Energy* **2019**, *38* (5), e13171
PANI/TiO_2 sodium persulfate	3.20 eV	J_{ph} = 12.10 μA/cm^2@1.68 V; IPCE = 10.07%@320	0.1 M NaOH	D. Hidalgo, S. Bocchini, M. Fontana, G. Saracco, S. Hernández, Green and low-cost synthesis of PANI·TiO_2 nanocomposite mesoporous films for photoelectrochemical water splitting. *RSC Adv.* **2015**, *5*, 49429−49438
PbS/Ro-GO/PANI/ITO	1.16 and 2 eV for PbS/Ro-GO/PANI	J_{ph} = 1.98 mA/cm^2, IPCE = 16.17%@390 nm	0.3 M $Na_2S_2O_3$	M. Shaban, M. Rabia, A.M. Abd El-Sayed, A. Ahmed, S. Sayed, Photocatalytic properties of PbS/graphene oxide/polyaniline electrode for hydrogen generation. *Sci. Rep.* **2017**, *7*, 14100
Au/PbS/Ro-GO/PANI		J_{ph} = 1.45 mA/cm^2, IPCE = 9.4%@390 nm		
PS/APS + FeCl3	1.95 eV	J_{ph} = 50 mA/cm^2, IPCE = 42%@307 nm	0.3 M KOH	in this work
copolymer PS/APS + FeCl3	2.5 eV	J_{ph} = 53 mA/cm^2, IPCE = 44%@307 nm		
polymer blend PS/APS + FeCl3	1.5 eV	J_{ph} = 65 mA/cm^2, IPCE = 46%@307 nm		

https://doi.org/10.1021/acsomega.1c01802
ACS Omega 2021, 6, 20779−20789

transferred to the CB of polyaniline. CPs are the promising ones that generate excited electrons when subject to visible light. Their bandgaps increase the PEC performance under visible light. Moreover, the conductivity of polyaniline stimulates the transfer of electrons during the creation of holes; hence, it decreases the photocorrosion of the semiconductor and improves the stability of the photoelectrode. The large active surface of polyaniline helps the reception of more incident light, thus facilitating the transfer of electrons to water molecules via an interfacial mechanism. Furthermore, the remaining holes are captured by the sacrificial reagent (KOH electrolyte). Polyaniline acts as a hole transport agent and averts the recombination of electrons and holes.[29] Finally, polyaniline transfers additional electrons to stimulate the reduction of H^+ to generate H_2.

3. EXPERIMENTAL SECTION

3.1. Materials. SA and aniline were provided by Merck Chemical Company (Germany). The chemical company El-Nasr Pharmaceutical provides chemically pure grades of concentrated hydrochloric acid (33%), methanol (99%), and acetone. Ammonium persulfate, ferric chloride, and dimethylformamide (DMF) were purchased from Sigma Aldrich Chemical Company (Germany). The pure ammonia solution (33%) was purchased from Prolabo-chemical Company (England). Double-distilled water is used as the medium for all polymerization reactions.

3.2. Synthesis of SA Oligomer. SA oligomers were synthesized by aqueous oxidative chemical polymerization of SA using APS, $FeCl_3$, and/or their mixture as an initiator under N_2 atmosphere for 48 h at 25 °C. SA solution (~0.001 mol, 1.73 g) dissolved in 100 mL of water/DMF (1:1) was polymerized in hydrochloric acid solution (0.04 mol L^{-1}) using the investigated oxidant (0.025 total moles) at 25 °C. Polysulfanilic acid was obtained by evaporation at 60 °C, washed with acetone, and then dried under vacuum at 60 °C.

3.3. Synthesis of Poly(aniline-*co*-sulfanilic acid) and PANI/SA Oligomer Blend. The copolymer was synthesized by addition of 1 mL of aniline to the above solution during the polymerization of SA dropwise over 30 min under stirring at 70 °C for 3 h and then left for 24 h. The obtained solution was evaporated at 60 °C, washed with acetone, and then dried under vacuum at 60 °C.

The polymer blend was synthesized by polymerization of 1 mL of aniline in 50 mL of aqueous solution of 0.5 g SA oligomer using the oxidant (0.025 total moles) at 25 °C for 48 h. The obtained solution was evaporated at 60 °C, washed with acetone, and then dried under vacuum at 60 °C.

3.4. Methodologies. All synthetic polymer samples were characterized by the following analytical tools, but only three samples prepared with APS (samples IV, V, and VI) were chosen to present based on clearing and resolution of the obtained figures.

3.4.1. UV–Visible and Infrared Spectroscopy. The UV spectra of these water-soluble polymer samples were performed using a Shimadzu dual-beam 2600 visible spectrophotometer, and the infrared measurement was performed using the Shimadzu FTIR Vertex 70 Bruker Optics technology. The above-mentioned spectral analysis was carried out in the Central Laboratory of Beni Suef University in Egypt.

3.4.2. X-ray Diffraction Patterns. The X-ray diffraction (XRD) pattern of the synthetic polymer sample was characterized with the Pananlytical Empryan 202964 X-ray diffractometer in the Central Laboratory of Beni Suf University, Egypt. The scanning range is 50−1400.

3.4.3. Electron Microscopy. Scanning electron microscopy (SEM) analysis was carried out using a JSM-6510LA scanning electron microscope, JEOL, Japan, at the Central Laboratory of Beni-Suef University, Egypt.

3.4.4. Gel Permeation Chromatography Analysis. Gel permeation chromatography (GPC) of synthetic samples used a Waters 515/2410 gel permeation chromatograph (Waters, USA) and ultra-hydraulic calibrated with poly(ethylene glycol) Standards and Series Refractive Index Detector 2410 Gel column, mobile phase: water, sodium nitrate (0.10 M), solvent: water, 0.05% sodium azide, flow rate: 1 mL/min, temperature 250° C, Egyptian Institute central laboratory of the oil.

3.5. Antimicrobial Activity. All synthetic polymer samples were introduced to investigation as antimicrobial polymers, but the samples (IV, V, and VI) show the best activity with respect to all the samples. Therefore, these polymeric fabrications were considered as the poor antimicrobial ones. The chosen three samples prepared by APS are present.

The agar diffusion technique was used to describe the antimicrobial activity of the polymer samples.[32] Polymer samples were tested against Gram-positive bacteria (*B. subtilis* ATCC 6633 and *S. aureus* ATCC 35556), Gram-negative bacteria (*E. coli* ATCC 23282 and *P. aeruginosa* ATCC 10145), yeast (Candida white IMRU 3669), and filamentous fungi (*A. niger* ATCC 16404). Bacteria and yeast grow on nutrient agar, while fungi grow on Czapek's Dox agar medium. The positive control bacteria are erythromycin, the fungus is metronidazole, and the yeast is nalidixic acid. All inspections were performed in duplicate, and the data listed are the average of the results obtained.

4. CONCLUSIONS

The chemical modification of low active materials was a target to introduce a new category of low-cost and active PEC catalysts. PS oligomers as antimicrobial and photoelectrocatalyst for water splitting to generate the H_2 fuel were enhanced by copolymerization with photoelectric active polyaniline. Different oxidants were used to optimize the quantity of the generated H_2 moles. The best oxidant was found to be a mixture of APS and $FeCl_3$ (1:1 mole ratio). Different PEC parameters were optimized such as monochromatic wavelength, electrode reusability, and stability. The PEC performance was evaluated using key indicators such as photocurrent density, conversion efficiency, and the number of hydrogen moles. The number of hydrogen moles was quantitively estimated to be 140.4, 160.2, and 300 μmol/h·g@−1 V for polymer, copolymer, and polymer blend in the presence of APS + $FeCl_3$ as an oxidant, respectively. Furthermore, the samples showed antibacterial activities against some hazardous bacteria such as *B. subtilis* ATCC 6633 Escherichia coli ATCC 23282 and *P. aeruginosa* ATCC 10145. Therefore, the present study overcomes many obstacles, including the rapid and steady killing of the harmful bacteria from wastewater, in addition to the efficient production of solar hydrogen fuel from the PEC water splitting through the synthesis of various new polymer-based photocatalysts.

https://doi.org/10.1021/acsomega.1c01802
ACS Omega 2021, 6, 20779−20789

■ ASSOCIATED CONTENT

Supporting Information

The Supporting Information is available free of charge at https://pubs.acs.org/doi/10.1021/acsomega.1c01802.

Characterization of different polymer samples (samples I, II, III, VII, VIII, and IX) including UV absorption, XRD, FTIR, and SEM in addition to the table of inhibition zone and MICs of hazardous species of bacteria (PDF)

■ AUTHOR INFORMATION

Corresponding Author

Fatma Mohamed − *Department of Chemistry, Faculty of Science and Nanophotonics and Applications Lab, Faculty of Science, Beni-Suef University, Beni-Suef 62514, Egypt;* orcid.org/0000-0002-1492-6256; Email: f_chem2010@yahoo.com

Authors

Reem M. Abdelfattah − *Department of Chemistry, Faculty of Science, Beni-Suef University, Beni-Suef 62514, Egypt*

Mohamed Shaban − *Nanophotonics and Applications Lab, Faculty of Science, Beni-Suef University, Beni-Suef 62514, Egypt; Department of Physics, Faculty of Science, Islamic University in Almadinah Almonawara, Almadinah 42351, Saudi Arabia*

Ahmed A.M. El-Reedy − *Basic Science Department, Faculty of Oral and Dental Medicine, Nahda University, Beni Suef 62514, Egypt*

Hanafy M. Abd El-Salam − *Department of Chemistry, Faculty of Science, Beni-Suef University, Beni-Suef 62514, Egypt*

Complete contact information is available at: https://pubs.acs.org/10.1021/acsomega.1c01802

Notes

The authors declare no competing financial interest.

■ ACKNOWLEDGMENTS

NA. No external funding is provided.

■ REFERENCES

(1) Abd El-Salam, H. M.; Azzam, E. M. S.; Aboad, R. S. Synthesis and characterization of poly(2- aminothiophenol-co-2-methylaniline)/silver nanoparticles as antisulfate-reducing bacteria. *Int. J. Polym. Mater. Polym. Biomater.* **2018**, *67*, 501−508.

(2) Pardieu, E.; Cheap, H.; Vedrine, C.; Lazerges, M.; Lattach, Y.; Garnier, F.; Remita, S.; Pernelle, C. Molecularly imprinted conducting polymer based electrochemical sensor for detection of atrazine. *Anal. Chim. Acta* **2009**, *649*, 236−245.

(3) Lu, G.; Wu, D.; Fu, R. Studies on the synthesis and antibacterial activities of polymeric quaternary ammonium salts from dimethylaminoethyl methacrylate. *React. Funct. Polym.* **2007**, *67*, 355−366.

(4) Abd El-Salam, H. M.; Mohamed, R. A.; Shokry, A. Facile polyacrylamide graft based on poly (2-chloroaniline) silver nanocomposites as antimicrobial. *Int. J. Polym. Mater. Polym. Biomater.* **2019**, *68*, 278−286.

(5) Kamel, E. M.; Ahmed, O. M.; Abd El-Salam, H. M. Fabrication of Facile Polymeric Nanocomposites Based On Chitosan-gr-P2-Aminothiophenol for Biomedical Applications. *Int. J. Biol. Macromol.* **2020**, *165*, 2649−2659.

(6) Maruthapandi, M.; Saravanan, A.; Luong, J. H. T.; Gedanken, A. Antimicrobial Properties of Polyaniline and Polypyrrole Decorated with Zinc-Doped Copper Oxide Microparticles. *Polymers* **2020**, *12*, 1286.

(7) Liao, C.-H.; Huang, C.-W.; Wu, J. C. S. Hydrogen Production from Semiconductor-based Photocatalysis via Water Splitting. *Catalysts* **2012**, *2*, 490−516.

(8) Thomas, C.; James, B. D.; Lomax, F. D., Jr; Kuhn, I. F., Jr. Fuel options for the fuel cell vehicle: hydrogen, methanol or gasoline? *Int. J. Hydrogen Energy* **2000**, *25*, 551−567.

(9) Wang, F.; Min, S.; Han, Y.; Feng, L. Visible-light-induced photocatalytic degradation of methylene blue with polyaniline-sensitized TiO2 composite photocatalysts. *Superlattices Microstruct.* **2010**, *48*, 170−180.

(10) Kondawar, S. B.; Acharya, S. A.; Dhakate, S. R. Microwave assisted hydrothermally synthesized nanostructure zinc oxide reinforced polyaniline nanocomposites. *Adv. Mater. Lett.* **2011**, *2*, 362−367.

(11) Katoch, A.; Burkhart, M.; Hwang, T.; Kim, S. S. Synthesis of polyaniline/TiO_2 hybrid nanoplates via a sol-gel chemical method. *Chem. Eng. J.* **2012**, *192*, 262−268.

(12) Guo, H.-x.; Lin, K.-l.; Zheng, Z.-s.; Xiao, F.-b.; Li, S.-x. Sulfanilic acid-modified P_25 TiO_2 nanoparticles with improved photocatalytic degradation on Congo red under visible light. *Dyes Pigm.* **2012**, *92*, 1278−1284.

(13) Alonso-Tellez, A.; Masson, R.; Robert, D.; Keller, N.; Keller, V. Comparison of Hombikat UV100 and P25 TiO_2 performance in gas-phase photocatalytic oxidation reactions. *J. Photochem. Photobiol., A* **2012**, *250*, 58−65.

(14) Dai, W.; Xu, H.; Yu, J.; Hu, X.; Luo, X.; Tu, X.; Yang, L. Photocatalytic reduction of CO_2 into methanol and ethanol over conducting polymers modified Bi_2WO_6 microspheres under visible light. *Appl. Surf. Sci.* **2015**, *356*, 173−180.

(15) Liu, L.; Ding, L.; Liu, Y.; An, W.; Lin, S.; Liang, Y.; Cui, W. A stable Ag_3PO_4@PANI core@shell hybrid: Enrichment photocatalytic degradation with π-π conjugation. *Appl. Catal., B* **2017**, *201*, 92−104.

(16) Wang, C.; Wang, L.; Jin, J.; Liu, J.; Li, Y.; Wu, M.; Chen, L.; Wang, B.; Yang, X.; Su, B.-L. Probing effective photocorrosion inhibition and highly improved photocatalytic hydrogen production on monodisperse PANI@CdS core-shell nanospheres. *Appl. Catal., B* **2016**, *188*, 351−359.

(17) Chitte, H. K.; Shinde, G. N.; Bhat, N. V.; Walunj, V. E. Synthesis of polypyrrole using ferric chloride ($FeCl_3$) as oxidant together with some dopants for use in gas sensors. *Sens. Technol.* **2011**, *01*, 47−56.

(18) Kim, J. H.; Kim, K. H.; Shin, J.; Lee, T. W.; Cho, M. J.; Choi, D. H. Electrical and photoelectrical properties of polymer single nanowire made of diketopyrrolopyrrole-based conjugated copolymer bearing dithieno[3,2-b:2,3-d]thiophene. *Synth. Met.* **2013**, *167*, 37−42.

(19) Ahmed, A. M.; Mohamed, F.; Ashraf, A. M.; Shaban, M.; Aslam Parwaz Khan, A.; Asiri, A. M. Enhanced photoelectrochemical water splitting activity of carbon nanotubes@TiO2 nanoribbons in different electrolytes. *Chemosphere* **2020**, *238*, 124554.

(20) Guo, X.-Z.; Luo, Y.-H.; Zhang, Y.-D.; Huang, X.-C.; Li, D.-M.; Meng, Q.-B. Study on the effect of measuring methods on incident photon-to-electron conversion efficiency of dye-sensitized solar cells by home-made setup. *Rev. Sci. Instrum.* **2010**, *81*, 103106.

(21) Ram, M. K.; Yavuz, Ö.; Lahsangah, V.; Aldissi, M. CO gas sensing from ultrathin nano-composite conducting polymer film. *Sens. Actuators, B* **2005**, *106*, 750−757.

(22) Attia, N. F.; Geckeler, K. E. Polyaniline−Polypyrrole Composites with Enhanced Hydrogen Storage Capacities. *Macromol. Rapid Commun.* **2013**, *34*, 931−937.

(23) Djara, R.; Lacour, M.-A.; Merzouki, A.; Cambedouzou, J.; Cornu, D.; Tingry, S.; Holade, Y. Iridium and Ruthenium Modified Polyaniline Polymer Leads to Nanostructured Electrocatalysts with High Performance Regarding Water Splitting. *Polym* **2021**, *13*, 190.

(24) Ganeshan, R.; Dhinasekaran, D.; Paramasivam, T.; Boukos, N.; Narayanan, V. Preparation and characterization of polyindole-iron oxide composite polymer electrolyte containing $LiClO_4$. *Polym.-Plast. Technol. Eng.* **2012**, *51*, 225−230.

(25) Kumar, A.; Pandey, A. C.; Prakash, R. Electro-oxidation of formic acid using polyindole-SnO_2 nanocomposite. *Catal. Sci. Technol.* **2012**, *2*, 2533−2538.
(26) Elimat, Z. M.; Zihlif, A. M.; Ragosta, G. Optical characterization of poly(ethylene oxide)/alumina composites. *Phys. B* **2010**, *405*, 3756−3760.
(27) Ahmed, A. M.; Abdalla, E. M.; Shaban, M. Simple and low-cost synthesis of Ba-doped CuO thin films for highly efficient solar generation of hydrogen. *J. Phys. Chem. C* **2020**, *124*, 22347−22356.
(28) Shaban, M.; El Sayed, A. M. Influence of the spin deposition parameters and La/Sn double doping on the structural, optical, and photoelectrocatalytic properties of $CoCo_2O_4$ photoelectrodes. *Sol. Energy Mater. Sol. Cells* **2020**, *217*, 110705.
(29) Shaban, M.; Hamd, A.; Amin, R. R.; Abukhadra, M. R.; Khalek, A. A.; Khan, A. A. P.; Asiri, A. M. Preparation and characterization of MCM-48/nickel oxide composite as an efficient and reusable catalyst for the assessment of photocatalytic activity. *Environ. Sci. Pollut. Res.* **2020**, *27*, 32670−32682.
(30) Helmy, A.; Rabia, M.; Shaban, M.; Ashraf, A. M.; Ahmed, S.; Ahmed, A. M. Graphite/rolled graphene oxide/carbon nanotube photoelectrode for water splitting of exhaust car solution. *Int. J. Energy Res.* **2020**, *44*, 7687−7697.
(31) Mohamed, F.; Rabia, M.; Shaban, M. Synthesis and characterization of biogenic iron oxides of different nanomorphologies from pomegranate peels for efficient solar hydrogen production. *J. Mater. Res. Technol.* **2020**, *9*, 4255−4271.
(32) Zhang, L.; Lang, Q.; Shi, Z. Electrochemical Synthesis of Three-Dimensional Polyaniline Network on 3-Aminobenzenesulfonic Acid Functionalized Glassy Carbon Electrode and Its Application. *Am. J. Anal. Chem.* **2010**, *01*, 102−112.

https://doi.org/10.1021/acsomega.1c01802
ACS Omega 2021, 6, 20779−20789